

# *Stratospheric ozone depletion and tropospheric ozone increases drive Southern Ocean interior warming*

Article

Accepted Version

Liu, W., Hegglin, M. I. ORCID: <https://orcid.org/0000-0003-2820-9044>, Checa-Garcia, R., Li, S., Gillett, N. P., Lyu, K., Zhang, X. and Swart, N. C. (2022) Stratospheric ozone depletion and tropospheric ozone increases drive Southern Ocean interior warming. *Nature Climate Change*, 12. pp. 365-372. ISSN 1758-678X doi: 10.1038/s41558-022-01320-w Available at <https://centaur.reading.ac.uk/104449/>

It is advisable to refer to the publisher's version if you intend to cite from the work. See [Guidance on citing](#).

To link to this article DOI: <http://dx.doi.org/10.1038/s41558-022-01320-w>

Publisher: Nature Publishing Group

All outputs in CentAUR are protected by Intellectual Property Rights law, including copyright law. Copyright and IPR is retained by the creators or other copyright holders. Terms and conditions for use of this material are defined in the [End User Agreement](#).

[www.reading.ac.uk/centaur](http://www.reading.ac.uk/centaur)

**CentAUR**

Central Archive at the University of Reading

Reading's research outputs online

**Stratospheric ozone depletion and tropospheric ozone increases drive Southern Ocean  
interior warming**

Wei Liu<sup>1</sup>, Michaela I. Hegglin<sup>2</sup>, Ramiro Checa-Garcia<sup>3</sup>, Shouwei Li<sup>1</sup>,  
Nathan P. Gillett<sup>4</sup>, Kewei Lyu<sup>5</sup>, Xuebin Zhang<sup>5</sup> and Neil C. Swart<sup>4</sup>

<sup>1</sup>Department of Earth and Planetary Sciences, University of California Riverside, Riverside, CA,  
USA

<sup>2</sup>Department of Meteorology, University of Reading, Whiteknights, Reading RG6 6BX, UK

<sup>3</sup>Institute of Meteorology and Climatology, University of Natural Resources and Life Sciences,  
Vienna, Austria

<sup>4</sup>Canadian Centre for Climate Modelling and Analysis, Environment and Climate Change Canada,  
Victoria, BC, Canada

<sup>5</sup>Centre for Southern Hemisphere Oceans Research, CSIRO Oceans and Atmosphere, Hobart,  
Tasmania, Australia

\*Corresponding Author: Wei Liu, address: Department of Earth and Planetary Sciences,  
University of California Riverside, 900 University Ave, Riverside, CA 92521.

Tel: 1-(951) 827-4508

Email address: [wei.liu@ucr.edu](mailto:wei.liu@ucr.edu)

Atmospheric ozone has undergone distinct changes in the stratosphere and troposphere during the second half of the twentieth century, with depletion in the stratosphere and an increase in the troposphere. Until now, the effect of these changes on ocean heat uptake has been unclear. Here we show that both stratospheric and tropospheric ozone changes have contributed to Southern Ocean interior warming, with the latter being more important. The ozone changes between 1955 and 2000 induced about 30% of the net simulated ocean heat content increase in the upper 2000 m of the Southern Ocean, with around 60% attributed to tropospheric increases and 40% to stratospheric depletion. Moreover, these two warming contributions show distinct physical mechanisms: Tropospheric ozone increases cause a subsurface warming in the Southern Ocean primarily via the deepening of isopycnals, while stratospheric ozone depletion via spiciness changes along isopycnals. Our results highlight that tropospheric ozone is more than an air pollutant and, as a greenhouse gas, has been pivotal to the Southern Ocean warming.

Atmospheric ozone has experienced distinct changes in the stratosphere and troposphere during the second half of the twentieth century. Notable ozone depletion has occurred in the stratosphere, most strikingly as the ozone hole over Antarctica, which has been attributed primarily to anthropogenic emissions of ozone-depleting substances<sup>1,2,3,4</sup>. In contrast, ozone increases in the troposphere have been observed (Extended Data Fig. 1) as a result of anthropogenic emissions of ozone precursors such as methane, non-methane volatile organic compounds, carbon monoxide and nitrogen oxides<sup>5,6,7,8</sup>. These atmospheric ozone changes have profound impacts on Earth's climate system. For example, stratospheric ozone depletion has significantly altered the tropospheric circulation by displacing the Southern Hemisphere westerly winds poleward during

austral summer<sup>9,10,11,12</sup>, though these Southern Hemisphere circulation trends paused around 2000 and are expected to reverse the sign owing to reduced emissions of ozone depleting substances following the signing of the Montreal Protocol and its Amendments<sup>13,14,15</sup>. By contrast, ozone impacts on oceans, especially those due to tropospheric ozone changes, are relatively less well explored.

The Fifth Assessment Report of the United Nations Intergovernmental Panel on Climate Change indicates that ozone constitutes the third-most important contribution to greenhouse gas forcing since pre-industrial times after carbon dioxide and methane<sup>16</sup>. Stratospheric and tropospheric ozone changes substantially modulate Earth's radiation balance<sup>17</sup>, and thus could also affect global ocean heat uptake. The role of the Southern Ocean is critical in the context of climate change as it is one of the most important regions for taking up excess heat in a warming climate<sup>18,19</sup>, and is markedly affected by Southern Hemisphere westerly winds<sup>20,21,22,23</sup>. During the past several decades, the Southern Ocean has shown a rapid subsurface warming<sup>24,25</sup>, only a small part of which, however, has been attributed to stratospheric ozone depletion<sup>26,27,28</sup>. Given the concurrent (but opposite) ozone changes in both the stratosphere and troposphere, one gap remains in our current knowledge of ozone-driven Southern Ocean warming: The impact of the increase in tropospheric ozone. Here, we employ historical simulations and accompanying ozone single-forcing experiments with a broad set of climate models from the Coupled Model Intercomparison Projects Phase 5/6 (CMIP5/6) to probe the mechanisms and impacts of stratospheric and tropospheric ozone changes on Southern Ocean interior warming during the second half of the twentieth century.

## Results

We first examine the ozone single-forcing experiments from the CMIP5 models in which the models were only forced with historical integrations of atmospheric ozone concentrations instead of all historical forcings (see Methods). These ozone single-forcing experiments demonstrate the effects of both stratospheric and tropospheric ozone changes together. Between 1955 and 2000, ozone depletion generates a strong stratospheric cooling trend in the Southern Hemisphere high latitudes (Extended Data Fig. 2), which leads to a poleward intensification of Southern Hemisphere westerly winds in the troposphere reminiscent of “annular mode-like” responses<sup>29</sup> (Fig. 1a). Along with the response in the atmosphere, ozone changes also produce a pronounced subsurface warming in the Southern Ocean. Within 40-50°S, the warming rate is larger than 0.01 K/decade in the upper 1000 m (Fig. 1c). When we integrate ocean heat content (OHC) over the upper 2000 m between 30°S and 60°S where ocean warming mainly occurs, we find a significant increase of OHC, with a trend of  $5.63 \pm 2.36$  ZJ/decade (1 ZJ =  $10^{21}$  joule; multi-model mean  $\pm$  1 standard deviation among models, see Methods) between 1955 and 2000 (Fig. 2a). Our results from these CMIP5 model simulations thus suggest a substantial Southern Ocean subsurface warming in response to stratospheric and tropospheric ozone changes.

We have also examined the recent ozone single-forcing experiments with the new generation of CMIP6 models. Unlike those with CMIP5 models, in these experiments CMIP6 models are forced with historical changes solely in stratospheric ozone concentration (see Methods). Hence the CMIP6 ozone experiments show solely the effect of stratospheric ozone change. Compared with the results from the CMIP5 experiments, the CMIP6 ozone experiments show similar stratospheric cooling in southern high latitudes and poleward intensified Southern Hemisphere

westerly winds, which indicates a major role of stratospheric ozone depletion in the atmospheric response during 1955-2000 (Fig. 1b). However, in the Southern Ocean, we find a much weaker subsurface warming in the CMIP6 stratospheric ozone only experiments with a pattern consistent with previous studies<sup>27,30</sup>. Between 40°S and 50°S, the warming rate is much smaller than 0.01 K/decade in the upper 2000 m (Fig. 1d). The upper 2000-m OHC between 30°S and 60°S exhibits a marginal increase between 1955 and 2000, with a trend of  $0.45 \pm 1.22$  ZJ/decade (multi-model mean  $\pm 1$  standard deviation among models; Fig. 2a). We further find no statistically significant difference in transient climate sensitivity between the CMIP5 and CMIP6 models (see Methods) but the Southern Ocean OHC trend in the CMIP5 simulations is one order of magnitude larger than that in the CMIP6 simulations, indicating that the difference in model climate sensitivity cannot serve as the major cause of such distinct warming trends in the Southern Ocean. On the other hand, the comparison between CMIP5 and CMIP6 model simulations implies that the tropospheric ozone increase is a key driver of Southern Ocean interior warming. Nevertheless, it is worth noting that this comparison cannot allow for a conclusive quantification of the impact nor shed light on the mechanism of tropospheric ozone increases on Southern Ocean warming, since the differences in prescribed historical ozone datasets between CMIP5 and CMIP6 models (Extended Data Fig. 1) and model responses to ozone forcing would need to be considered.

### **Quantifying the ozone impacts on Southern Ocean warming**

To quantify the impact of tropospheric ozone change on Southern Ocean interior warming and investigate the mechanism, we employ two ensembles of ozone single-forcing simulations performed with the same climate model, CanESM5. This model simulates a Southern Ocean

warming generally in alignment with the ensemble mean result of CMIP6 stratospheric ozone only experiments (Fig. 2a). The first CanESM5 ensemble is forced with historical changes in both stratospheric and tropospheric ozone, equivalent to the CMIP5 simulations described above but adopting the CMIP6 simulation protocol<sup>31,32</sup>. The second ensemble simulation is equivalent to the CMIP6 ozone experiments described above in which the model is forced with historical integrations of solely stratospheric ozone changes (see Methods). The difference between the two ensemble simulations therefore isolates the effect of tropospheric ozone change. Relative to preindustrial times, we find that both ensemble experiments from CanESM5 simulate a stratospheric cooling in the southern high latitudes and a significant poleward intensification of Southern Hemisphere westerlies in the troposphere between 1955 and 2000 (Fig. 3a,b). On the other hand, tropospheric ozone increases lead to a warming in the troposphere and a cooling in the stratosphere<sup>33</sup> (Extended Data Fig. 3), together with a significant upward intensification of Southern Hemisphere westerly winds in the upper levels and a poleward intensification of westerly winds towards surface (Fig. 3c). These tropospheric-ozone-produced atmosphere temperature and circulation changes are comparable to those induced by stratospheric ozone depletion towards the surface layers, suggesting that tropospheric ozone changes could potentially have considerable impacts on the oceans underneath.

We further probe the temperature response in the Southern Ocean in the two CanESM5 ensemble simulations. We find a region of pronounced warming extending downward and equatorward to the north of 60°S as a response to the combined stratospheric and tropospheric ozone changes. Between 40°S and 50°S, this tongue of warming waters reaches 1200 m with a warming rate exceeding 0.01 K/decade (Fig. 3d). Part of this subsurface warming is induced by stratospheric



ozone depletion, which is, however, mostly limited to the upper 600 m (Fig. 3e). On the other hand, the vertical extension of the tongue of warming waters depends essentially on tropospheric ozone forcing. The increase of tropospheric ozone creates such a deep warming in the Southern Ocean that warming larger than 0.01 K/decade is found to penetrate as deep as 1000 m within 40-50°S (Fig. 3f). To the north of the tongue of warming waters, there is a tongue of cooling waters in the upper levels of the Southern Ocean, which results principally from stratospheric ozone depletion and secondarily from tropospheric ozone increases (Fig. 3e,f). A similar cooling feature is found at high latitudes south of 55°S (Fig. 3d,f). It is worth noting that the warming pattern due to tropospheric ozone increases is different from that due to the rising well-mixed greenhouse gases such as carbon dioxide. The rise of well-mixed greenhouse gases induces ubiquitous while vertically decaying warming in the upper 2000-m ocean in the Southern Ocean<sup>20,21,27,34</sup>.

Here we estimate the OHC variations in the upper 2000 m between 30°S and 60°S in the two sets of CanESM5 simulations. We find that atmospheric ozone changes induce a robust upward OHC trend of  $4.58 \pm 3.35$  ZJ/decade (ensemble mean  $\pm 1$  standard deviation among ensembles) between 1955 and 2000, of which about two-fifths ( $1.84 \pm 2.50$  ZJ/decade, ensemble mean  $\pm 1$  standard deviation among ensembles) can be attributed to stratospheric ozone depletion while the other three-fifths (2.74 ZJ/decade, the difference of the ensemble means between the two suites of ozone simulations) is driven by tropospheric ozone increases. Our results confirm the importance of tropospheric ozone to Southern Ocean heat uptake and storage. Importantly, the increases in tropospheric ozone have been more effective in driving the interior warming over the Southern Ocean during the second half of the twentieth century compared to stratospheric ozone depletion.

Moreover, to set in context the effect of ozone forcing on the historical OHC increase in the Southern Ocean over the 1955-2000 period, we compare OHC changes in the upper 2000 m within 30-60°S between the CanESM5 historical simulations that also include the other greenhouse gas forcings from carbon dioxide, methane and nitrous oxide and the combined stratosphere-troposphere ozone single-forcing experiment (Fig. 2b). We find that CanESM5 simulates a general long-term increase of OHC in the Southern Ocean, at a rate of  $13.77 \pm 4.29$  ZJ/decade (ensemble mean  $\pm 1$  standard deviation among ensembles) between 1955 and 2000, which is consistent with the OHC trends inferred from observations (16.25 ZJ/decade) and CMIP5 models ( $14.60 \pm 5.27$  ZJ/decade, multi-model mean  $\pm 1$  standard deviation among models) (Fig. 2b). Using the CanESM5 ozone experiment, we further find that about 33.2% of the net historical OHC increase between 1955 and 2000 is caused by atmospheric (both stratospheric and tropospheric) ozone changes. This ratio is in line with that suggested by the historical CMIP5 model ozone experiment ( $38.4 \pm 10.4\%$ , multi-model mean  $\pm 1$  standard deviation among models).

### **Physical mechanisms of ozone-driven Southern Ocean warming**

To further understand the mechanisms by which stratospheric and tropospheric ozone changes drive Southern Ocean interior warming, we decompose the temperature and salinity changes between 1955 and 2000 at depth levels into the spiciness changes along isopycnals and heave-related changes owing to the vertical heave of isopycnals<sup>35</sup> (see Methods). The spiciness reveals alterations in water mass properties as a result of the subduction of surface temperature and salinity anomalies and changes by interior mixing processes. The heave of isopycnals could

be linked to changes in wind-driven ocean circulation and the redistribution of heat and salt in the interior ocean<sup>36</sup>.

We first depict the temperature and salinity responses to total atmospheric ozone variations. During 1955-2000, the zonally averaged spiciness changes on density surfaces exhibit strong warming and salification trends in the upper ocean toward isopycnal outcrops, especially in the latitudes between 40°S and 60°S (Fig. 4a,b). These warming and salification trends primarily result from stratospheric ozone depletion and not from tropospheric ozone increases (Fig. 4c,d). Between 40°S and 60°S, the Southern Ocean takes heat from the atmosphere but loses freshwater in response to stratospheric ozone depletion (Fig. 5a,b), both contributing to warming and salification spiciness trends<sup>36</sup>. The peak of Southern Ocean surface heat uptake is around 55°S (Extended Data Fig. 4), essentially due to the increase of downward turbulent latent heat flux<sup>37</sup> over the Indian Ocean sector (Extended Data Fig. 5). Increases in surface shortwave radiation fluxes also contribute to Southern Ocean heat uptake in these latitudes (Extended Data Fig. 3). On the other hand, the reduction in surface freshwater flux can be mostly attributed to changes in precipitation minus evaporation (P-E) to the north of 54°S but is likely related to sea-ice variations to the south (Extended Data Fig. 6). Between 40°S and 54°S, the P-E reduction results from both precipitation decreases and evaporation increases and is especially robust over the Pacific sector (Extended Data Fig. 7).

Besides the warming and salification trends in the isopycnal outcropping region between 40°S and 60°S, we also find cooling and freshening spiciness changes to the north of 40°S on density surfaces between 26.3 and 27.0 kg/m<sup>3</sup> (Fig. 4a,b), within the density ranges of the Subantarctic

Mode Water (SAMW) and Antarctic Intermediate Water (AAIW) simulated by climate models<sup>38</sup>. Particularly, the spiciness changes in the AAIW density range (26.7-27.0 kg/m<sup>3</sup>) can be attributed mostly to stratospheric ozone depletion (Fig. 4c,d) while those in the SAMW density range (26.3-26.6 kg/m<sup>3</sup>) mainly to tropospheric ozone increases (Fig. 4e,f). These ozone-induced cooling signals contribute to the cooling trend found at corresponding locations from observations and historical simulations during 1955-2000 (Extended Data Fig. 8).

After remapping the spiciness changes onto depth levels using the mean depth of each density surface, we find the major spiciness warming (>0.01 K/decade) trends in response to total atmospheric ozone variations extending equatorward and downward from the surface layer at 60°S to about 600 m at 40°S (Fig. 6a). The stratospheric ozone depletion is responsible for most of the ozone-induced warming trends in the upper 500 m (Fig. 6c) while tropospheric ozone increases primarily account for the spiciness warming below (Fig. 6e).

We further analyze the heave component of Southern Ocean temperature change. We find a subsurface warming region (>0.01 K/decade) extending equatorward between 36°S and 51°S and downward in 300-1100 m (Fig. 6b) in response to atmospheric ozone changes, accompanied by a cooling tongue to the north and in upper levels. This pair of warming and cooling anomalies has been linked to poleward intensified surface westerly winds and indicates heat redistribution within the Southern Ocean<sup>21,39</sup>. Specifically, stratospheric ozone depletion drives an intensification of surface westerly winds at and to the south of the Antarctic Circumpolar Current but a relaxation to the north (Fig. 5c, Extended Data Fig. 9), in a pattern consistent with other CMIP6 models (Extended Data Fig. 10). The zonally averaged zonal wind change exhibits a

dipole-like pattern, with positive and negative anomalies to the south and north of around 50°S. The resultant anomalous Ekman transport convergence and wind-driven downwelling produces a deepening of isopycnals in the latitudes around 50°S and hence heave-induced changes of warming. While to the north of about 43°S, the weakening of surface westerlies progressively decays, which prompts an anomalous Ekman transport divergence and wind-driven upwelling (Extended Data Fig. 9d) and thus leads to shallower isopycnals and cooling heave changes in these latitudes (Fig. 6d).

Tropospheric ozone increases, on the other hand, engender different changes in surface winds from those due to stratospheric ozone depletion (Fig. 5c, Extended Data Fig. 9). The zonally averaged surface zonal wind change also reflects a dipole-like pattern but located more northward, with positive and negative anomalies occurring to the south and north of around 42°S. This pattern indicates less poleward displaced surface westerlies than their counterparts driven by stratospheric ozone depletion. Tropospheric ozone increases also drive poleward-intensified Southern Hemisphere precipitation and significantly increase evaporation at lower latitudes where the tropospheric ozone increases are stronger (Extended Data Fig. 6f). In the ocean, the wind-driven Ekman pumping (Extended Data Fig. 9d) produces isopycnals deepening in much lower latitudes, around 42°S, and warming heave changes there (Fig. 6f). These heave-related warming changes are much stronger than those induced by stratospheric ozone depletion, which is likely due to the fact that the oceanic thermocline is more strongly stratified at lower latitudes<sup>36</sup>, allowing the wind-driven downwelling more effectively to create warming heave changes there.

## Discussion

In summary, we have examined the climate impacts of atmospheric ozone changes during the second half of the twentieth century, with a focus on disentangling effects of stratospheric ozone depletion and tropospheric ozone increases. We show that while stratospheric ozone depletion plays a dominant role in atmospheric temperature and wind changes in southern high latitudes in the stratosphere and upper levels of the troposphere, tropospheric ozone increases have made a larger contribution to Southern Ocean interior warming. Between 1955 and 2000, about one-third of the historical OHC increase in the upper 2000 m of the Southern Ocean between 30°S and 60°S was induced by atmospheric ozone changes, of which around three-fifths can be attributed to tropospheric ozone increases and the other two-fifths to stratospheric ozone depletion. Tropospheric ozone increases cause Southern Ocean subsurface warming primarily via the deepening of isopycnals. They give rise to an intensification of surface westerly winds over the Southern Ocean such that the wind-driven Ekman pumping brings about isopycnal deepening around 42°S and prompts heave-induced warming there. On the other hand, stratospheric ozone depletion promotes warming in the Southern Ocean mainly through spiciness changes along isopycnals in the upper 500 m. In response to stratospheric ozone depletion, the net surface downward heat flux increases but the freshwater flux decreases over the Southern Ocean between 40°S and 60°S, contributing to the warming and salification spiciness changes in the isopycnal outcropping regions of the Southern Ocean.

In our study, the finding that stratospheric and tropospheric ozone changes contributed to around one-third of the historical OHC increase during the second half of the twentieth century is consistent with the result from previous studies examining simulations with fixed ozone

depleting substances (ODSs)<sup>40</sup>. However, the response to ODSs, inferred by differencing historical simulations with all anthropogenic forcings and simulations with fixed ODSs, omits changes in tropospheric ozone induced by precursor omissions, but includes radiative effects of ODSs themselves, and hence these results are not directly comparable with our study of the direct effects of tropospheric and stratospheric ozone changes. Furthermore, our results suggest that, when the effect of tropospheric ozone increases is considered, the ozone impacts on Southern Ocean interior warming are much larger than previous estimates that only considered stratospheric ozone depletion<sup>27</sup>. Between 1955 and 2000, tropospheric ozone increases significantly affect the P-E over the Southern Ocean. As such, our results highlight that tropospheric ozone, besides being an air pollutant, is an important contributor to ocean heat uptake and hydrological cycle change in the Southern Hemisphere.

## Main References

1. Farman, J.C. Gardiner, B.G. & Shanklin J.D. Large losses of total ozone in Antarctica reveal seasonal ClO<sub>x</sub>/NO<sub>x</sub> interaction. *Nature*, **315**, 207-210 (1985).
2. Rowland, F.S. Chlorofluorocarbons and the depletion of stratospheric ozone. *Am. Sci.*, **77**, 36-45 (1989).

3. Solomon, S. Progress towards a quantitative understanding of Antarctic ozone depletion. *Nature*, **347**, 347-354 (1990).
4. WMO (World Meteorological Organization), Scientific Assessment of Ozone Depletion: 2018, Global Ozone Research and Monitoring Project – Report No. 58, 588 pp., Geneva, Switzerland (2018).
5. Young, P.J., Naik, V., Fiore, A.M., Gaudel, A., Guo, J., Lin, M.Y., Neu, J.L., Parrish, D.D., Rieder, H.E., Schnell, J.L., Tilmes, S., Wild, O., Zhang, L., Ziemke, J., Brandt, J., Delcloo, A., Doherty, R.M., Geels, C., Hegglin, M.I., Hu, L., Im, U., Kumar, R., Luhar, A., Murray, L., Plummer, D., Rodriguez, J., Saiz-Lopez, A., Schultz, M.G., Woodhouse, M.T. & Zeng, G. Tropospheric Ozone Assessment Report: Assessment of global-scale model performance for global and regional ozone distributions, variability, and trends. *Elementa: Sci. Anthropol.*, **6**, 10 (2018).
6. Stevenson, D. S., Young, P. J., Naik, V., Lamarque, J.-F., Shindell, D. T., Voulgarakis, A., Skeie, R. B., Dalsoren, S. B., Myhre, G., Berntsen, T. K., Folberth, G. A., Rumbold, S. T., Collins, W. J., MacKenzie, I. A., Doherty, R. M., Zeng, G., van Noije, T. P. C., Strunk, A., Bergmann, D., Cameron-Smith, P., Plummer, D. A., Strode, S. A., Horowitz, L., Lee, Y. H., Szopa, S., Sudo, K., Nagashima, T., Josse, B., Cionni, I., Righi, M., Eyring, V., Conley, A., Bowman, K. W., Wild, O. & Archibald, A. Tropospheric ozone changes, radiative forcing and attribution to emissions in the Atmospheric Chemistry and Climate Model Inter-comparison Project (ACCMIP). *Atmos. Chem. Phys.*, **13**, 3063-3085 (2013).
7. Cooper, O.R., Parrish, D.D., Ziemke, J., Balashov, N.V., Cupeiro, M., Galbally, I.E., Gilge, S., Horowitz, L., Jensen, N.R., Lamarque, J.F. & Naik, V. Global distribution and trends of



- tropospheric ozone: An observation-based review. *Elementa: Sci. Anthropol.*, **2**, 000029 (2014).
8. Yeung, L.Y., Murray, L.T., Martinerie, P., Witrant, E., Hu, H., Banerjee, A., Orsi, A. & Chappellaz, J. Isotopic constraint on the twentieth-century increase in tropospheric ozone. *Nature*, **570**, 224–227 (2019).
9. Thompson, D.W. & Solomon, S. Interpretation of recent Southern Hemisphere climate change. *Science*, **296**, 895–899 (2002).
10. Son, S.W., Polvani, L.M., Waugh, D.W., Akiyoshi, H., Garcia, R., Kinnison, D., Pawson, S., Rozanov, E., Shepherd, T.G. & Shibata, K. The impact of stratospheric ozone recovery on the Southern Hemisphere westerly jet. *Science*, **320**, 1486–1489 (2008).
11. Polvani, L.M., Waugh, D.W., Correa, G.J. & Son, S.W. Stratospheric ozone depletion: The main driver of twentieth-century atmospheric circulation changes in the Southern Hemisphere. *J. Clim.*, **24**, 795–812 (2011).
12. Eyring, V., Arblaster, J.M., Cionni, I., Sedláček, J., Perlwitz, J., Young, P.J., Bekki, S., Bergmann, D., Cameron-Smith, P., Collins, W.J., Faluvegi, G., Gottschaldt, K.-D., Horowitz, L.W., Kinnison, D.E., Lamarque, J.-F. Marsh D.R., Saint-Martin, D., Shindell, D.T., Sudo, K., Szopa, S. & Watanabe, S. Long-term ozone changes and associated climate impacts in CMIP5 simulations. *J. Geophys. Res.: Atmos*, **118**, 5029–5060 (2013).
13. Arblaster, J., Meehl, G. & Karoly, D. Future climate change in the Southern Hemisphere: Competing effects of ozone and greenhouse gases. *Geophys. Res. Lett.*, **38**, L02701 (2011).
14. McLandress, C., Shepherd, T.G., Scinocca, J.F., Plummer, D.A., Sigmond, M., Jonsson, A.I. & Reader, M.C. Separating the dynamical effects of climate change and ozone depletion. Part II: Southern Hemisphere troposphere. *J. Clim.*, **24**, 1850–1868 (2011).

15. Banerjee, A., Fyfe, J.C., Polvani, L.M., Waugh, D. & Chang, K.L. A pause in Southern Hemisphere circulation trends due to the Montreal Protocol. *Nature*, **579**, 544-548 (2020).
16. Myhre, G., Shindell, D., Bréon, F.-M., Collins, W., Fuglestedt, J., Huang, J., Koch, D., Lamarque, J.-F., Lee, D., Mendoza, B., Nakajima, T., Robock, A., Stephens, G., Takemura, T. & Zhang H. Anthropogenic and Natural Radiative Forcing. In: Climate Change 2013: The Physical Science Basis. Contribution of Working Group I to the Fifth Assessment Report of the Intergovernmental Panel on Climate Change [Stocker, T.F., D. Qin, G.-K. Plattner, M. Tignor, S.K. Allen, J. Boschung, A. Nauels, Y. Xia, V. Bex and P.M. Midgley (eds.)]. Cambridge University Press, Cambridge, United Kingdom and New York, NY, USA (2013).
17. Checa-Garcia, R., Hegglin, M.I., Kinnison, D., Plummer, D.A. & Shine, K.P. Historical tropospheric and stratospheric ozone radiative forcing using the CMIP6 database. *Geophys. Res. Lett.*, **45**, 3264–3273 (2018).
18. Gregory, J.M. Vertical heat transports in the ocean and their effect on time-dependent climate change. *Clim. Dyn.*, **16**, 501-515 (2000).
19. Frölicher, T.L., Sarmiento, J.L., Paynter, D.J., Dunne, J.P., Krasting, J.P. & Winton, M. Dominance of the Southern Ocean in anthropogenic carbon and heat uptake in CMIP5 models. *J. Clim.*, **28**, 862-886 (2015).
20. Fyfe, J.C., Saenko, O.A., Zickfeld, K., Eby, M. & Weaver, A.J. The role of poleward-intensifying winds on Southern Ocean warming. *J. Clim.*, **20**, 5391–5400 (2007).
21. Liu, W., Lu, J., Xie, S.-P. & Fedorov, A. Southern Ocean heat uptake, redistribution, and storage in a warming climate: The role of meridional overturning circulation. *J. Clim.*, **31**, 4727–4743 (2018).

22. Waugh, D.W., McC. Hogg, A., Spence, P., England, M.H. & Haine, T.W. Response of Southern Ocean ventilation to changes in midlatitude westerly winds. *J. Clim.*, **32**, 5345-5361 (2019).
23. Li, Q., England, M.H. & McC. Hogg, A. Transient Response of the Southern Ocean to Idealized Wind and Thermal Forcing across Different Model Resolutions. *J. Clim.*, **34**, 5477-5496 (2021).
24. Gille, S.T. Warming of the Southern Ocean since the 1950s. *Science*, **295**, 1275–1277 (2002).
25. Durack, P.J., Gleckler, P.J., Landerer, F.W. & Taylor, K.E. Quantifying underestimates of long-term upper-ocean warming. *Nat. Clim. Change*, **4**, 999–1005 (2014).
26. Sigmond, M., Reader, M.C., Fyfe, J.C. & Gillett, N.P. Drivers of past and future Southern Ocean change: Stratospheric ozone versus greenhouse gas impacts. *Geophys. Res. Lett.*, **38**, L12 601 (2011).
27. Swart, N.C., Gille, S.T., Fyfe, J.C. & Gillett, N.P. Recent Southern Ocean warming and freshening driven by greenhouse gas emissions and ozone depletion. *Nat. Geosci.*, **11**, 836–841 (2018).
28. Li, S., Liu, W., Lyu, K. & Zhang, X. The effects of historical ozone changes on Southern Ocean heat uptake and storage. *Clim. Dyn.*, **57**, 2269–2285 (2021)
29. Ring, M. J. & Plumb, R. A. The Response of a Simplified GCM to Axisymmetric Forcings: Applicability of the Fluctuation–Dissipation Theorem. *J. Atmos. Sci.*, **65**, 3880-3898 (2008).
30. Bitz, C.M. & Polvani, L.M. Antarctic climate response to stratospheric ozone depletion in a fine resolution ocean climate model. *Geophys. Res. Lett.*, **39**, L20705 (2012).

31. Waliser, D., Gleckler, P. J., Ferraro, R., Taylor, K. E., Ames, S., Biard, J., Bosilovich, M. G., Brown, O., Chepfer, H., Cinquini, L., Durack, P. J., Eyring, V., Mathieu, P.-P., Lee, T., Pinnock, S., Potter, G. L., Rixen, M., Saunders, R., Schulz, J., Thépaut, J.-N., & Tuma, M.: Observations for Model Intercomparison Project (Obs4MIPs): status for CMIP6. *Geosci. Model Dev.*, **13**, 2945–2958 (2020).
32. Eyring, V., Bony, S., Meehl, G.A., Senior, C.A., Stevens, B., Stouffer, R.J. & Taylor, K.E. Overview of the Coupled Model Intercomparison Project Phase 6 (CMIP6) experimental design and organization. *Geosci. Model Dev.*, **9**, 1937-1958 (2016).
33. Seidel, D.J., Gillett, N.P., Lanzante, J.R., Shine, K.P. & Thorne, P.W. Stratospheric temperature trends: our evolving understanding. *WIREs Clim. Change*, **2**, 592-616 (2011).
34. Shi, J.R., Talley, L.D., Xie, S.P., Liu, W. & Gille, S.T. Effects of Buoyancy and Wind Forcing on Southern Ocean Climate Change. *J. Clim.*, **33**, 10003-10020 (2020).
35. Bindoff, N.L. & McDougall T.J. Diagnosing climate change and ocean ventilation using hydrographic data. *J. Phys. Oceanogr.*, **24**, 1137–1152 (1994).
36. Lyu, K., Zhang, X., Church, J.A & Wu, Q. Processes responsible for the Southern Hemisphere ocean heat uptake and redistribution under anthropogenic warming. *J. Clim.*, **33**, 3787–3807 (2020).
37. Zhang, L. & Cooke, W. Simulated changes of the Southern Ocean air-sea heat flux feedback in a warmer climate. *Clim. Dyn.*, **56**, 1–16 (2021).
38. Sallée, J.B., Shuckburgh, E., Bruneau, N., Meijers, A.J., Bracegirdle, T.J., Wang, Z. & Roy, T. Assessment of Southern Ocean water mass circulation and characteristics in CMIP5 models: Historical bias and forcing response. *J. Geophys. Res.: Oceans*, **118**, 1830–1844 (2013).

39. Cai, W., Cowan, T., Godfrey, S. & Wijffels, S. Simulations of processes associated with the fast warming rate of the southern midlatitude ocean. *J. Clim.*, **23**, 197-206 (2010).
40. Solomon, A., Polvani, L.M., Smith, K.L. & Abernathey, R.P. The impact of ozone depleting substances on the circulation, temperature, and salinity of the Southern Ocean: An attribution study with CESM1(WACCM). *Geophys. Res. Lett.*, **42**, 5547–5555 (2015).

## Acknowledgments

W.L. is supported by the Alfred P. Sloan Foundation as a Research Fellow and by U.S. National Science Foundation (AGS-2053121, OCE 2123422). K.L. and X.Z. are funded by the Centre for Southern Hemisphere Oceans Research (CSHOR), jointly funded by the Qingdao National Laboratory for Marine Science and Technology (QNLN, China) and the Commonwealth Scientific and Industrial Research Organisation (CSIRO, Australia).

## Author Contributions Statement

W.L. conceived the study, performed the analysis and wrote the original draft of the manuscript. S.L. contributed to the analysis. W.L., M.I.H., R.C.-G., S.L., N.P.G., K.L., X.Z. and N.C.S. contributed to interpreting the results and made substantial improvements to the manuscript.

## Competing Interests Statement

The authors declare no competing interests.

## Figure legends

**Figure 1. Changes in Southern Hemisphere westerlies and Southern Ocean temperature in response to ozone changes in CMIP5 and CMIP6 simulations.** (top row) Trends of annual and zonal mean zonal winds during 1955-2000 (shading in m/s/decade) of the multi-model means (MMMs) from (a) CMIP5 and (b) CMIP6 models ozone single-forcing experiments. The annual climatologies of zonal mean zonal winds (contour in m/s, with an interval of 5 m/s and the zero contours thickened) of the MMMs from CMIP5 and CMIP6 models preindustrial control runs are superimposed on both panels, respectively. (bottom row) Trends of annual and zonal ocean temperature during 1955-2000 (shading in K/decade) of the MMMs from (c) CMIP5 and (d) CMIP6 models ozone single-forcing experiments. Stippling indicates that the change is statistically insignificant at the 95% confidence level of the Mann-Kendall trend significance test (see Methods).

**Figure 2. Observed and simulated Southern Ocean heat content.** (a) Ocean heat content (OHC) anomalies (relative to the value in 1955) integrated over the upper 2000 m between 30°S and 60°S from ozone single-forcing experiments with four CMIP5 models (MMM, medium blue; inter-model spread, light blue; see Methods) and four CMIP6 models (MMM, magenta; inter-model spread, light magenta), and the ensemble means from CanESM5 stratospheric and tropospheric ozone experiment (blue), stratospheric ozone only experiment (red) as well as the difference between the two (black) indicating the effect of tropospheric ozone change. The inter-model spread is calculated as one standard deviation of the ensemble means of individual models. (b) Same as panel (a) but for OHC anomalies from the IAP observation data (orange) and historical simulations with the four CMIP5 models (MMM, medium purple; inter-model spread, light purple) and CanESM5 (ensemble mean, purple). OHC anomalies from CMIP5

ozone single-forcing experiments are also included in the panel. Note that the OHC from the IAP observations is a single realization, which has larger interannual variations than the other OHCs from MMM.

**Figure 3. Changes in Southern Hemisphere westerlies and Southern Ocean temperature in response to ozone changes in CanESM5 simulations.** (top row) Changes in annual and zonal mean zonal winds (shading in m/s) during 1955-2000 (relative to preindustrial control run) for the ensemble means in CanESM5 (a) stratospheric and tropospheric ozone experiment and (b) stratospheric ozone only experiment as well as (c) the difference between the two indicating the effect of tropospheric ozone change. Stippling indicates that the change is statistically insignificant at the 95% confidence level of the Student's t-test (see Methods). (bottom row) Same as the top row but for trends of annual and zonal mean ocean temperature during 1955-2000 (shading in K/decade). Stippling indicates that the change is statistically insignificant at the 95% confidence level of the Mann-Kendall trend significance test (see Methods).

**Figure 4. Temperature and salinity spiciness changes on density surfaces in CanESM5 ozone experiments.** (left column) Spiciness changes in annual and zonal mean ocean temperature trends during 1955-2000 (shading in K/decade) on density surfaces for the ensemble means in CanESM5 (a) stratospheric and tropospheric ozone experiment and (c) stratospheric ozone only experiment as well as (e) the difference between the two indicating the effect of tropospheric ozone change. (right column) Same as the left column but for spiciness changes in annual and zonal mean ocean salinity trends (shading in  $10^{-2}$  psu/decade).

**Figure 5. Surface heat flux, freshwater flux and zonal winds changes in CanESM5 ozone experiments.** (a) Changes in annual and zonal mean net surface heat fluxes over the Southern Ocean during 1955-2000 (relative to preindustrial control run) for the ensemble means in CanESM5 stratospheric and tropospheric ozone experiment (light blue; significant, blue) and stratospheric ozone only experiment (orange; significant, red) as well as the difference between the two (gray; significant, black) indicating the effect of tropospheric ozone change. Panels (b) and (c) are the same as (a) but for changes in annual and zonal mean net surface freshwater fluxes over the ocean and surface zonal winds. The variable of surface zonal wind is obtained from atmosphere model outputs and land is then masked out for the variable so that winds are on the liquid ocean water surface in most parts of the Southern Ocean but on sea ice surface around or south of 60°S where sea ice exists. Heat and freshwater fluxes are positive downward. In all the panels, changes are tested based on the Student's t-test and denoted statistically significant when exceeding the 95% confidence level (see Methods).

**Figure 6. Spiciness and heave changes of ocean temperature in CanESM5 ozone experiments.** (left column) Spiciness changes in annual and zonal mean ocean temperature trends during 1955-2000 (shading in K/decade) above 2000 m but below the mixed layer (~150 m) in the Southern Ocean for the ensemble means in CanESM5 (a) stratospheric and tropospheric ozone experiment and (c) stratospheric ozone only experiment as well as (e) the difference between the two indicating the effect of tropospheric ozone change. (right column) Same as the left column but for heave changes.

## Methods



## Observations

To evaluate the performance of CanESM5 in simulating the historical warming in the Southern Ocean during the second half of the twentieth century, we use one objectively analyzed ocean dataset, the Institute of Atmospheric Physics (IAP) ocean temperature analysis<sup>41</sup>. The IAP ocean temperature analysis has global ocean coverage of 1-degree horizontal resolution on 41 vertical levels from the surface down to 2000 m. It has a monthly resolution from 1940 to the present. This ocean temperature analysis minimizes the errors from ocean sampling by *in situ* observations and allows for accurate estimates of regional and global OHC changes during the past several decades, especially those in the Southern Ocean.

## CMIP5 and CMIP6 preindustrial control, historical and ozone single-forcing simulations

We use the preindustrial control runs of four CMIP5 (CCSM4, CESM1-CAM5, FGOALS-g2 and GISS-E2-H) and four CMIP6 (CanESM5, GISS-E2-1-G, IPSL-CM6A-LR and MIROC6) models. For either CMIP5 or CMIP6, the four-model ensemble has an average transient climate response (TCR)<sup>42,43,44</sup> that is very close to the mean TCR reported by previous studies<sup>43,44</sup>, suggesting that the models we used can well represent the transient climate sensitivity of the models of either generation. For all the models except CESM1-CAM5 and GISS-E2-1-G, we estimate each model's climate drift in ocean temperatures as a 500-year temperature trend (during the last 500 years) in each model's preindustrial control run. As CESM1-CAM5 and GISS-E2-1-G only have 320 and 345 years of simulation available in the CMIP5 and CMIP6 archives, for either model, we estimate its climate drift in ocean temperature as the temperature trend during the last 200 years of the preindustrial control run. For CanESM5 and GISS-E2-1-G, the preindustrial simulations of “p1” and “f2” are adopted to be consistent with their ozone

experiments, respectively. We remove climate drifts from the trends of ocean temperatures in the historical and ozone single-forcing simulations with these CMIP5 and CMIP6 models. We also remove the climate drift in ocean salinity for CanESM5 (the salinity trend of its preindustrial control run) when conducting the spiciness and heave decomposition.

The CMIP5 historical simulations are performed including all the natural and anthropogenic forcings during the historical period. The CMIP5 ozone single-forcing experiments on the other hand are forced by stratospheric and tropospheric ozone only during the historical period while the other forcings are fixed at their preindustrial levels<sup>45</sup>. In the four CMIP5 models, the ozone chemistries are either semi-offline calculated or prescribed<sup>12</sup>. In this study, we adopt 11 ensemble members of ozone single-forcing (stratospheric and tropospheric ozone) experiments (2 from CCSM4, 3 from CESM1-CAM5, 1 from FGOALS-g2 and 5 from GISS-E2-H) and 21 ensemble members of historical simulations with the four CMIP5 models (6 from CCSM4, 4 from CESM1-CAM5, 5 from FGOALS-g2 and 6 from GISS-E2-H). Note here, for CCSM4 ozone experiment, there are three ensemble members while temperature outputs in 2000-2005 are not available for one member in the CMIP5 archives; so only the other two ensemble members are used. For CCSM4 and GISS-E2-H preindustrial and historical simulations, ensembles of “p1” perturbation are adopted to be consistent with the perturbation in the ozone experiments. We calculate the ensemble mean for each model and then calculate the multi-model mean (MMM) based on the ensemble means of the four models to minimize the effects of internal climate variability and model differences. The inter-model difference is estimated as one standard deviation of the ensemble means of the models.

The ozone single-forcing experiments with CMIP6 models are akin to their historical simulations but forced by stratospheric ozone variations only. For models without coupled chemistry, they prescribe the same stratospheric ozone concentrations as used in their historical simulations<sup>46</sup>. For models with coupled chemistry, their chemistry schemes are turned off. Note here, that while these model configurations neglect to represent potential feedbacks of changing dynamics on the ozone fields in a self-consistent way, we consider such effects to be of second-order relevance. Such an assumption is justified given that the climate response, for example, the response of the polar vortex breakdown to equivalent effective stratospheric chlorine, does not show a systematic difference between models with prescribed and interactive ozone<sup>47</sup>.

The CMIP6 models prescribe the ensemble mean monthly mean three-dimensional stratospheric ozone concentrations as simulated in their historical runs but have fixed three-dimensional long-term monthly mean tropospheric ozone concentrations from their preindustrial control runs. In particular, grid cells are categorized tropospheric when they have an ozone concentration below 100 ppbv (parts per billion by volume) in the climatology of the preindustrial control run. This definition of the troposphere is consistent throughout the historical period and facilitates inter-model comparisons<sup>48</sup>. Albeit the tropopause height may alter with climate change, several studies<sup>6,17</sup> suggest that the tropopause choice only has a marginal effect on radiative forcing. To examine the ozone impacts on Southern Ocean interior warming during the second half of the twentieth century, we adopt 28 ensemble members of ozone single-forcing (stratospheric ozone only) experiments with the four CMIP6 models (10 from CanESM5, 5 from GISS-E2-1-G, 10 from IPSL-CM6A-LR and 3 from MIROC6) and calculate the MMM and inter-model difference of the CMIP6 models.

Besides, we compare the transient climate responses (TCRs) between CMIP5 and CMIP6 models. For CMIP5 models<sup>42,43</sup>, the TCRs of CCSM4, CESM1-CAM5, FGOALS-g2 and GISS-E2-H are 1.7 K, 2.33 K, 1.4 K and 1.7 K, so their average TCR is 1.78 K. For CMIP6 models<sup>44</sup>, the TCRs of CanESM5, GISS-E2-1-G, IPSL-CM6A-LR and MIROC6 are 2.66 K, 1.68 K, 2.32 K and 1.52 K, so their average TCR is 2.05 K. Both averages are very close to the mean TCRs reported by previous studies<sup>43,44</sup> based on 29 CMIP5 models and 34 CMIP6 models, respectively. This result suggests that, for either CMIP5 or CMIP6, the four-model ensemble well represents the transient climate sensitivity of the models of either generation. The Student's t-test result further shows that the difference of TCR between CMIP5 and CMIP6 model means is insignificant at the 95% confidence level, which suggests that there is no statistically significant difference in transient climate sensitivity between the CMIP5 and CMIP6 models used in the current study.

### **CanESM5 and associated simulations**

CanESM5 is a fully coupled climate model participating in CMIP6<sup>49</sup>. The atmosphere component is the Canadian Atmosphere Model (CanAM5), which employs a spectral dynamical core with a T63 truncation (an approximate 2.8-degree horizontal resolution) and a hybrid sigma-pressure coordinate with 49 vertical layers up to about 1 hPa. The land component incorporates the Canadian Land Surface Scheme (CLASS) and the Canadian Terrestrial Ecosystem Model (CTEM). The ocean component is a modified version of the Nucleus for European Modelling of the Ocean model (NEMO), which includes ocean biogeochemistry represented by the Canadian Model of Ocean Carbon (CMOC) and employs a ~1-degree

horizontal resolution and 45 vertical levels. The Louvain-la-Neuve sea-Ice Model version 2 (LIM2) also operates within the NEMO framework.

A 25-member historical simulation labeled as perturbed physics member 1 (“p1”) has been performed with CanESM5 during 1850-2014. Individual ensemble members are initialized at different years from preindustrial control run and perturbed by the conservative remapping wind-stress fields. We use these 25 ensembles of CanESM5 historical simulation as they share the same perturbation scheme (“p1”) with CanESM5 ozone simulations. We compare the trend of zonal mean temperature in the ensemble mean of the CanESM5 historical simulation with that in the IAP data during 1955-2000 and find that the CanESM5 historical simulation is able to well capture the observed warming tongue ( $>0.03$  K/decade) in the upper 1000 m between  $40^{\circ}\text{S}$  and  $50^{\circ}\text{S}$  (Extended Data Fig. 8). This result demonstrates the model fidelity in simulating the Southern Ocean temperature response to external climate forcings.

Besides the 10-ensemble stratospheric ozone only experiment as in line with several other CMIP6 models, CanESM5 provides a 10-ensemble member historical total ozone-only experiment in which the model prescribes the monthly mean three-dimensional ozone concentrations from the historical simulation through the depth of the atmosphere. This total ozone-only experiment is consistent with the CMIP5 ozone single-forcing (stratospheric and tropospheric ozone) experiments. We adopt the simulations of this pair of ozone experiments to isolate and quantify the effects of stratospheric and tropospheric ozone on Southern Ocean interior warming.

### **The spiciness and heave decomposition**

The spiciness and heave decomposition follows previous studies<sup>35,36</sup>. For changes in potential temperature ( $\theta$ ) and salinity ( $S$ ) at depth  $z$ , i.e.,  $\theta'|_z$  and  $S'|_z$ , they can be decomposed as:

$$\theta'|_z \cong \theta'|_n + N'\theta_z \quad (1)$$

$$S'|_z \cong S'|_n + N'S_z \quad (2)$$

where  $\theta'|_n$  and  $S'|_n$  denote the spiciness changes of temperature and salinity that are density-compensating along neutral density surfaces;  $N'\theta_z$  and  $N'S_z$  denote the heave changes of temperature and salinity that are related to the neutral density surface height change  $N'$  (positive downward).

### **The OHC calculation**

At each location, the OHC within a layer between the depths  $z_1$  and  $z_2$  is calculated as

$$OHC = \rho_0 C_p \int_{z_1}^{z_2} \theta dz \quad (3)$$

where  $\rho_0$  denotes sea water density and  $C_p$  denotes the specific heat capacity of sea water.

### **The statistical significance test**

We examine the statistical significance of climate response to ozone forcing in CanESM5 based on the Student's t-test. We divide 500 years of CanESM5 preindustrial simulation into 10 truncations and treat each truncation as one ensemble member. Hence we construct 10 preindustrial ensembles with non-overlapping 50-year periods. We apply the Student's t-test to the three pairs of ensemble simulations—total-ozone versus preindustrial, stratospheric-ozone versus preindustrial and total-ozone versus stratospheric-ozone—to estimate the statistical significance of total, stratospheric and tropospheric ozone effects. Besides, we examine the

statistical significances of trends of CMIP5 and CMIP6 MMMs and CanESM5 ensemble means based on the Mann-Kendall trend significance test.

#### **Data availability**

All the raw CMIP5 model simulation data are publically available at

<https://esgf-node.llnl.gov/search/cmip5/>

All the raw CMIP6 model simulation data are publically available at

<https://esgf-node.llnl.gov/projects/cmip6/>

The IAP observation data are publically available at

<http://www.ocean.iap.ac.cn/>

#### **Code availability**

Figures are generated via the NCAR Command Language (NCL, Version 6.5.0) [Software].

(2018). Boulder, Colorado: UCAR/NCAR/CISL/TDD. <http://dx.doi.org/10.5065/D6WD3XH5>

The codes and processed variables to generate Figures 1-6 are available at Zenodo<sup>50</sup>.

#### **Methods References**

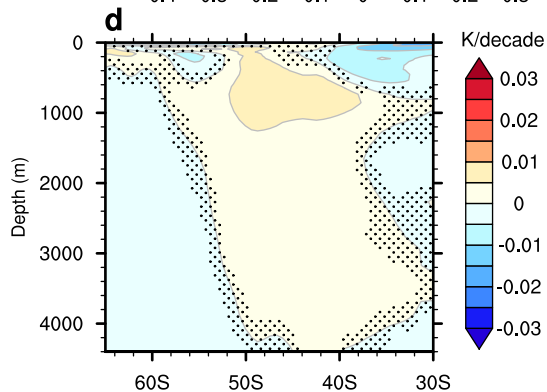
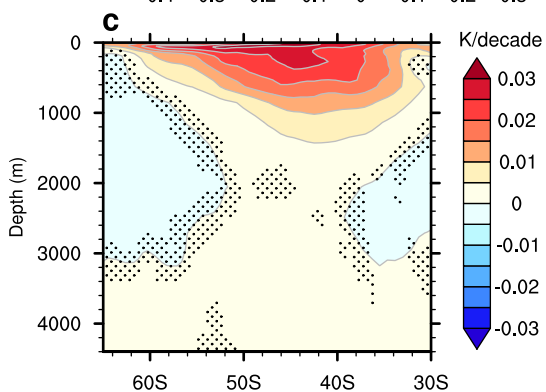
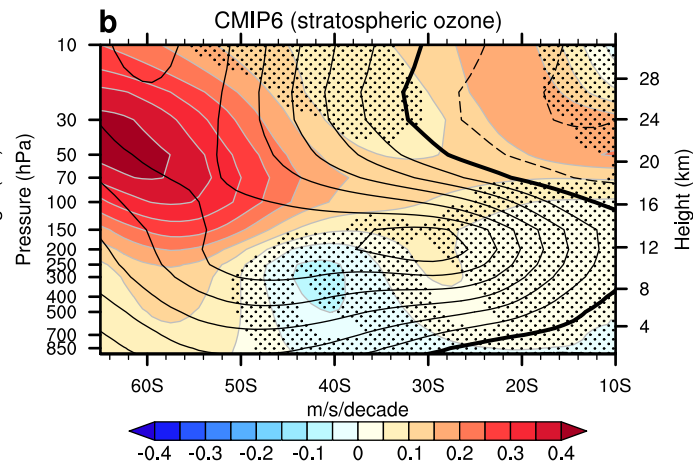
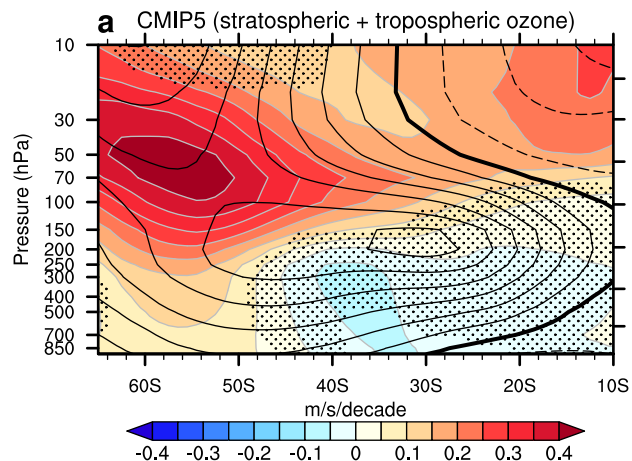
41. Cheng, L., Trenberth, K.E., Fasullo, J., Boyer, T., Abraham, J. & Zhu, J. Improved estimates of ocean heat content from 1960 to 2015. *Sci. Adv.*, **3**, e1601545 (2017).

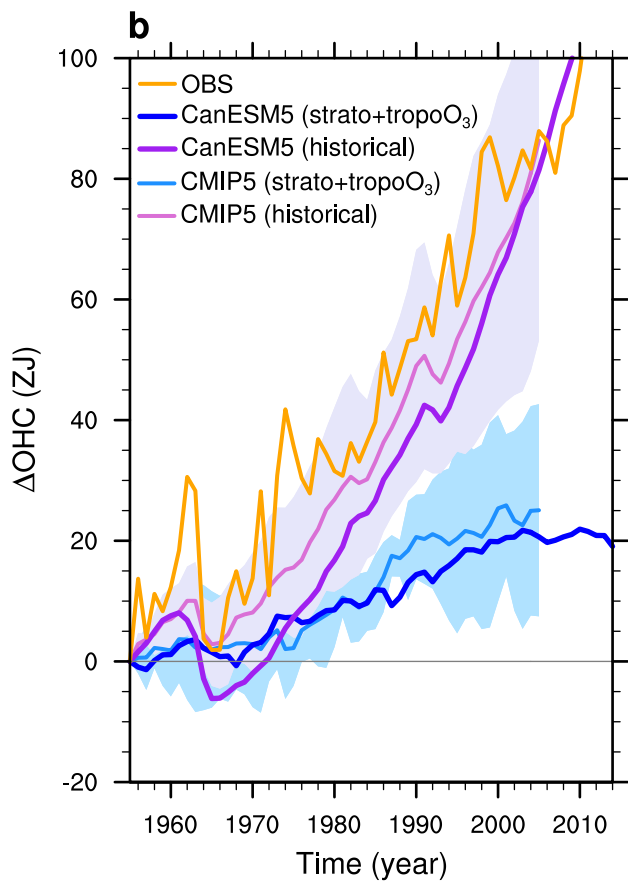
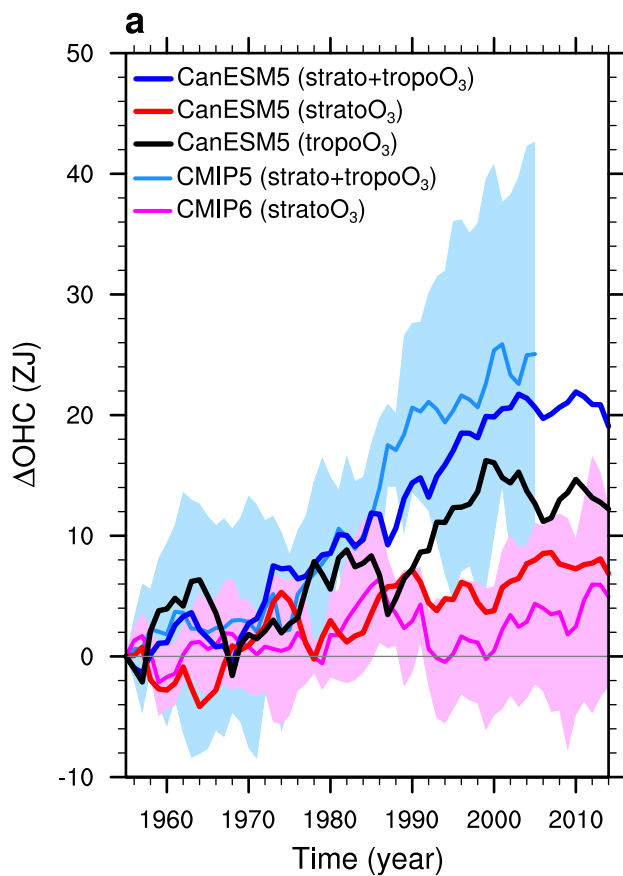
42. Meehl, G.A., Washington, W.M., Arblaster, J.M., Hu, A., Teng, H., Kay, J.E., Gettelman, A., Lawrence, D.M., Sanderson, B.M. & Strand, W.G. Climate change projections in CESM1 (CAM5) compared to CCSM4. *J. Clim.*, **26**, 6287-6308 (2013).

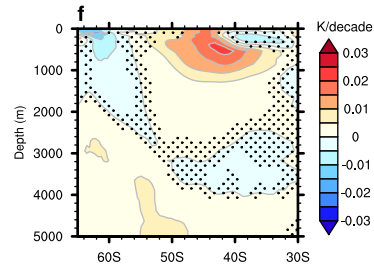
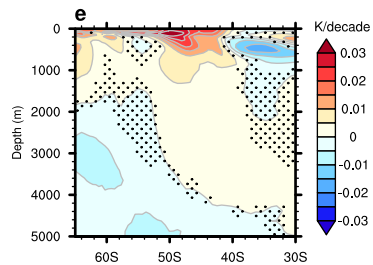
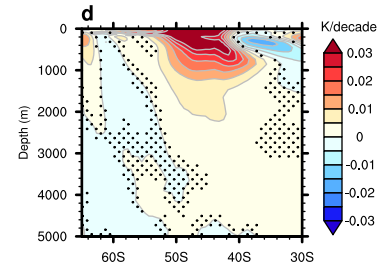
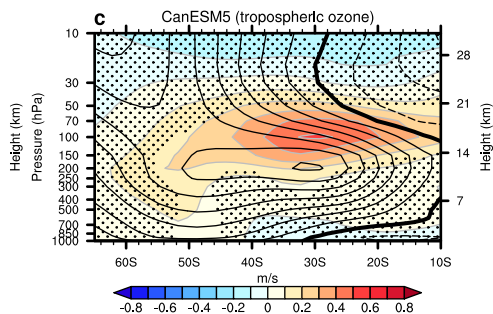
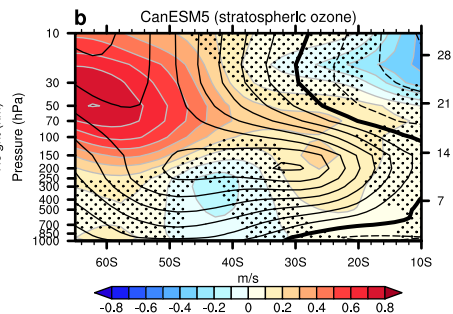
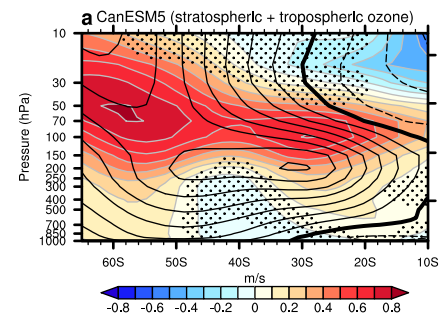
43. Meehl, G.A., Senior, C.A., Eyring, V., Flato, G., Lamarque, J.F., Stouffer, R.J., Taylor, K.E. & Schlund, M. Context for interpreting equilibrium climate sensitivity and transient climate response from the CMIP6 Earth system models. *Sci. Adv.*, **6**, eaba1981 (2020).
44. Nijse, F.J., Cox, P.M. & Williamson, M.S. Emergent constraints on transient climate response (TCR) and equilibrium climate sensitivity (ECS) from historical warming in CMIP5 and CMIP6 models. *Earth Syst. Dyn.*, **11**, 737-750 (2020).
45. Xia, Y., Huang, Y. & Hu, Y. On the climate impacts of upper tropospheric and lower stratospheric ozone. *J. Geophys. Res.: Atmos.*, **123**, 730–739 (2018).
46. Gillett, N.P., Shiogama, H., Funke, B., Hegerl, G., Knutti, R., Matthes, K., Santer, B.D., Stone, D. & Tebaldi, C. The Detection and Attribution Model Intercomparison Project (DAMIP v1.0) contribution to CMIP6. *Geosci. Model Dev.*, **9**, 3685–3697 (2016).
47. Mindlin, J., Shepherd, T. G., Vera, C. & Osman, M. Combined effects of global warming and ozone depletion recovery on Southern Hemisphere atmospheric circulation and regional precipitation. *Geophys. Res. Lett.*, **48**, e2021GL092568 (2021).
48. Young, P. J., Archibald, A. T., Bowman, K. W., Lamarque, J.-F., Naik, V., Stevenson, D. S., Tilmes, S., Voulgarakis, A., Wild, O., Bergmann, D., Cameron-Smith, P., Cionni, I., Collins, W. J., Dalsøren, S. B., Doherty, R. M., Eyring, V., Faluvegi, G., Horowitz, L. W., Josse, B., Lee, Y. H., MacKenzie, I. A., Nagashima, T., Plummer, D. A., Righi, M., Rumbold, S. T., Skeie, R. B., Shindell, D. T., Strode, S. A., Sudo, K., Szopa, S. & Zeng, G. Pre-industrial to end 21st century projections of tropospheric ozone from the Atmospheric Chemistry and Climate Model Intercomparison Project (ACCMIP). *Atmos. Chem. Phys.*, **13**, 2063–2090 (2013).

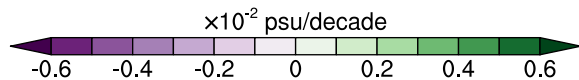
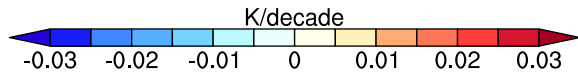
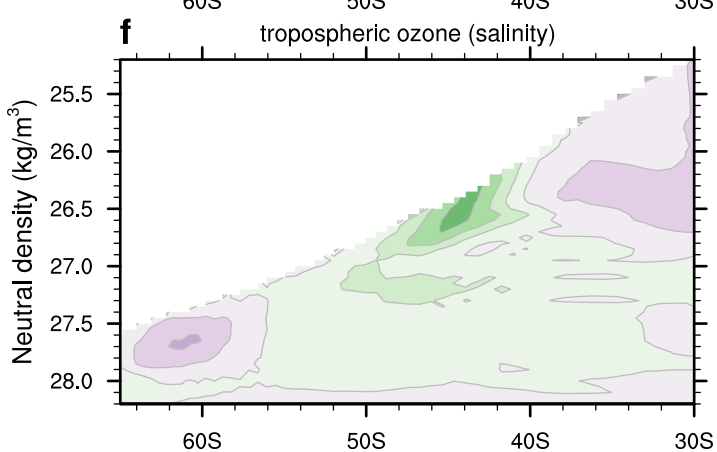
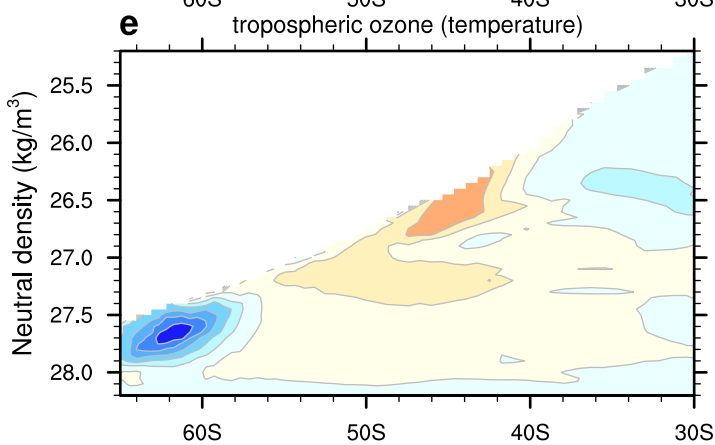
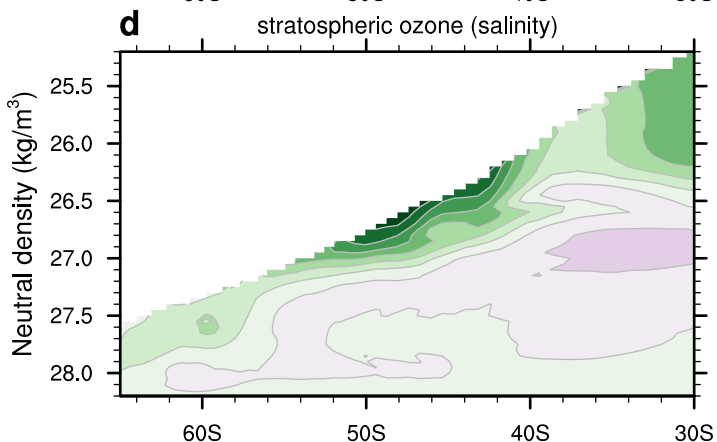
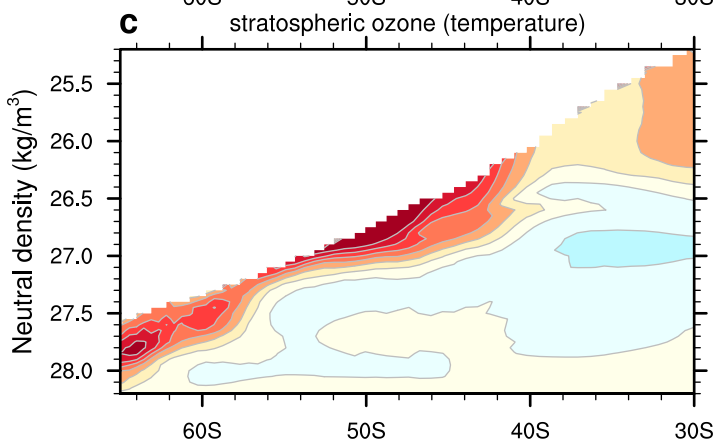
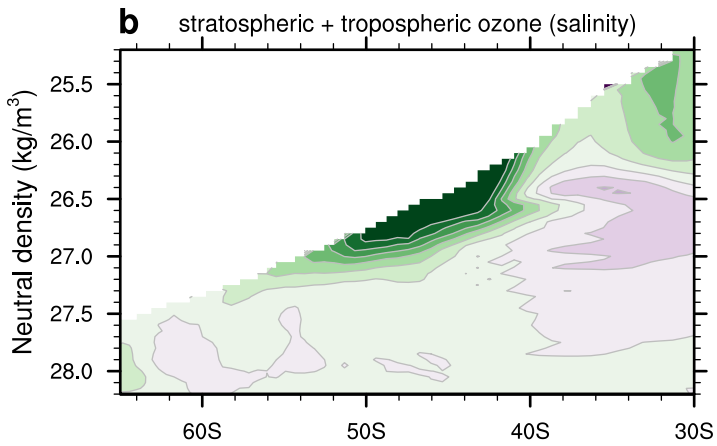
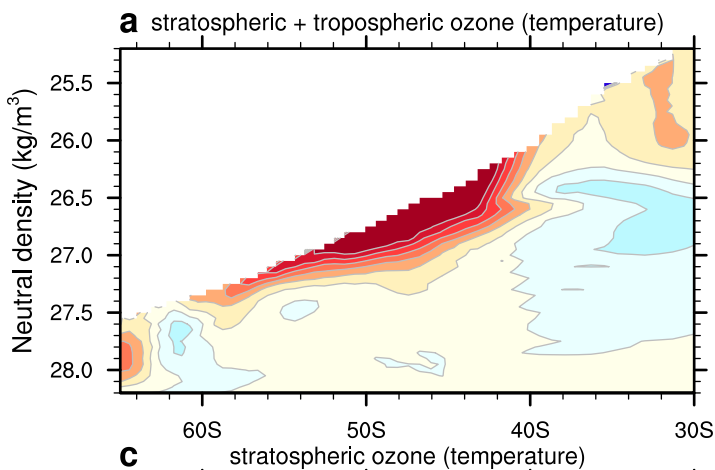


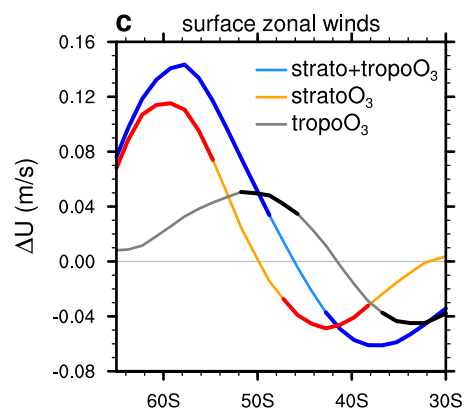
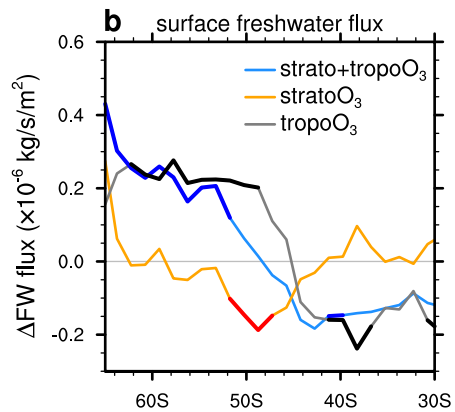
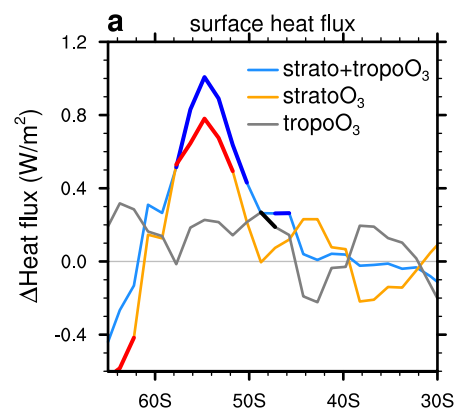
- 686 49. Swart, N. C., Cole, J. N. S., Kharin, V. V., Lazare, M., Scinocca, J. F., Gillett, N. P., Anstey,  
687 J., Arora, V., Christian, J. R., Hanna, S., Jiao, Y., Lee, W. G., Majaess, F., Saenko, O. A.,  
688 Seiler, C., Seinen, C., Shao, A., Sigmond, M., Solheim, L., von Salzen, K., Yang, D. &  
689 Winter, B. The Canadian Earth System Model version 5 (CanESM5.0.3). *Geosci. Model*  
690 *Dev.*, **12**, 4823–4873 (2019).
- 691 50. Liu, W., Hegglin, M., Checa-Garcia, R., Li, S., Gillett, N., Lyu, K., Zhang, X., & Swart, N.  
692 Stratospheric ozone depletion and tropospheric ozone increases drive Southern Ocean  
693 interior warming [Data set]. Zenodo. <https://doi.org/10.5281/zenodo.6003088> (2022).

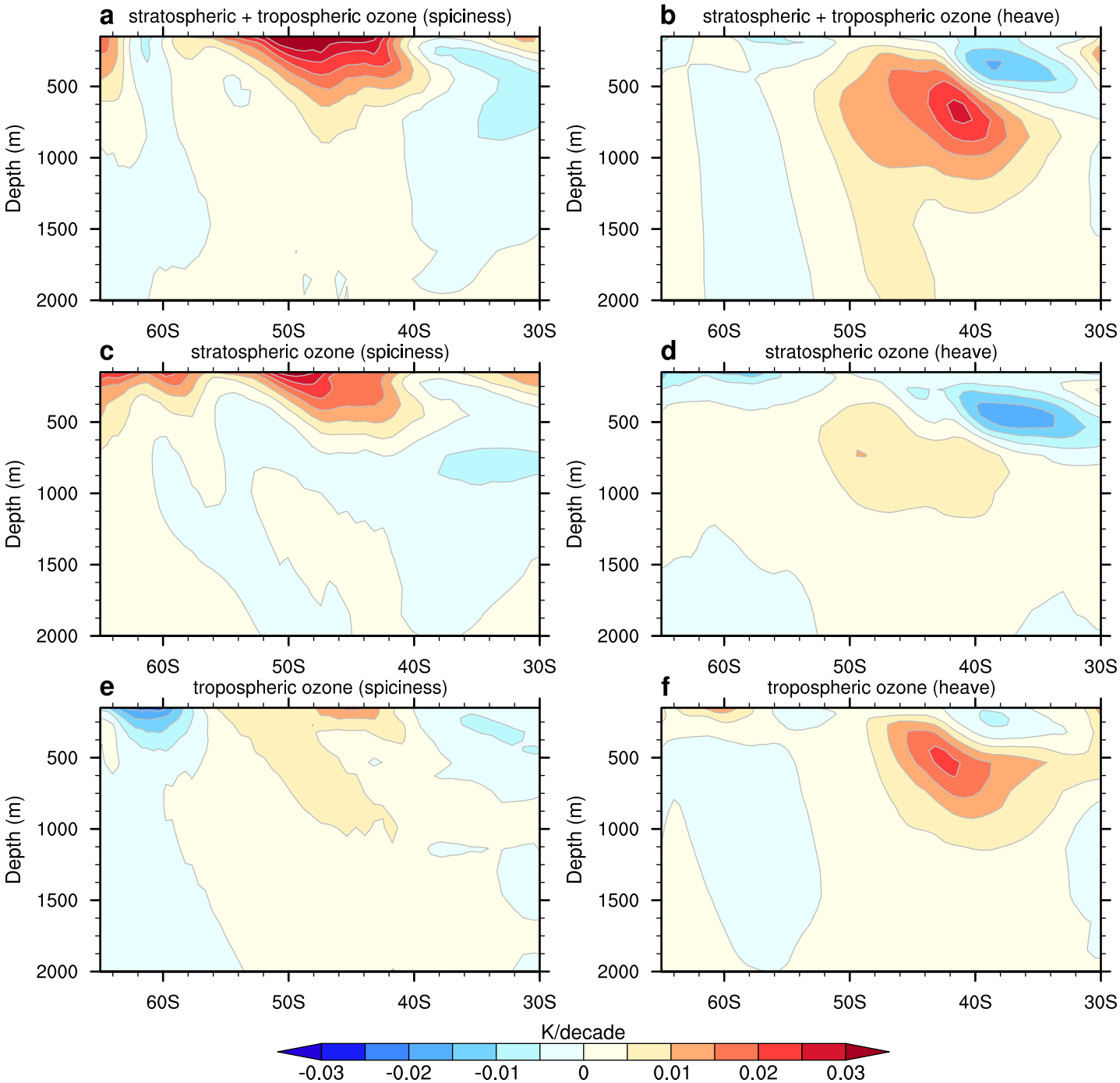


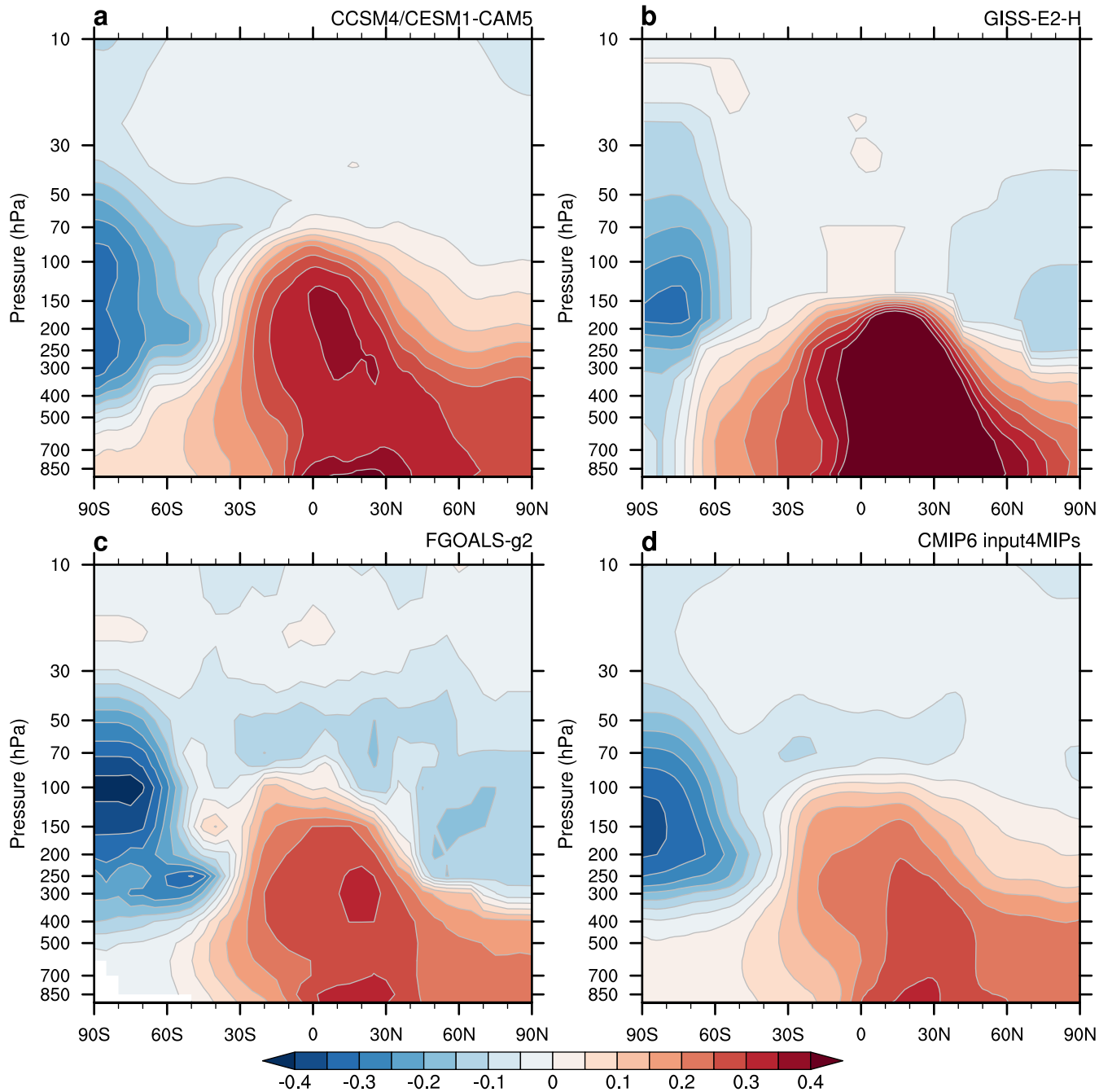




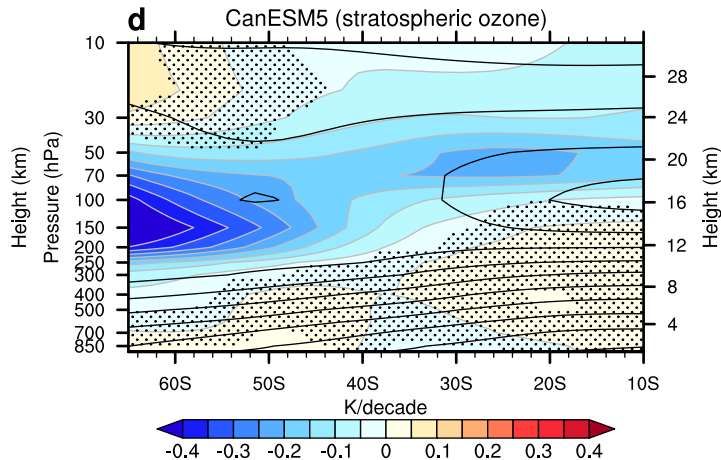
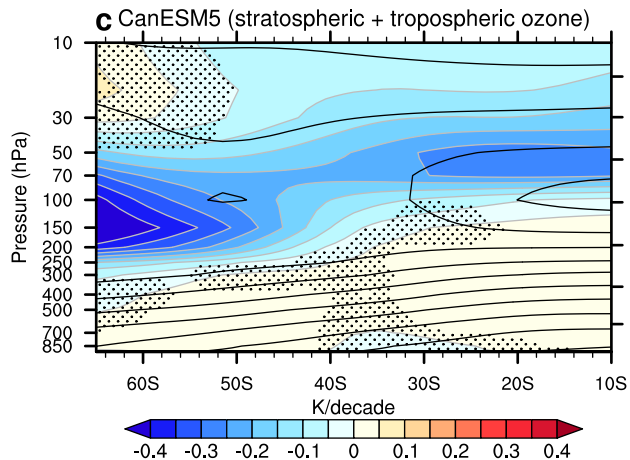
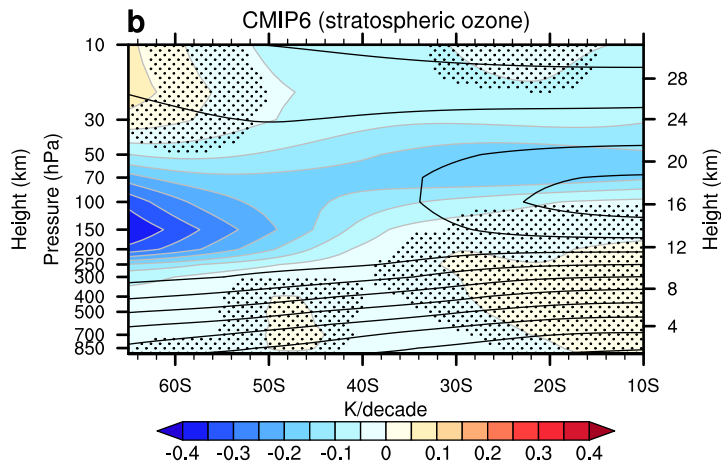
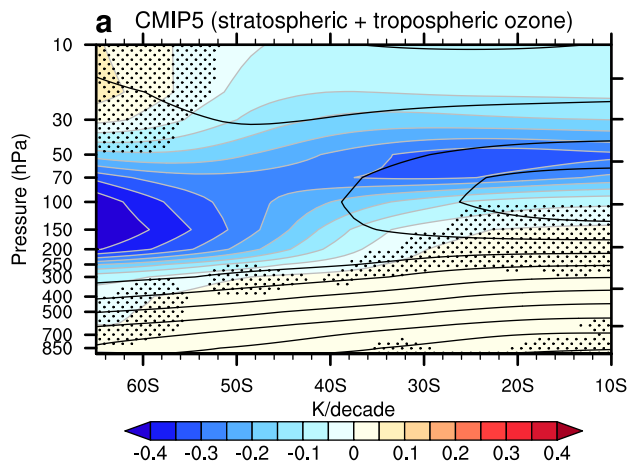


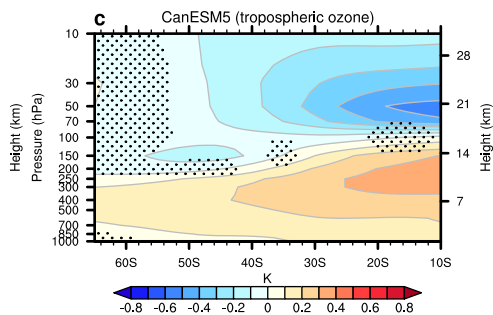
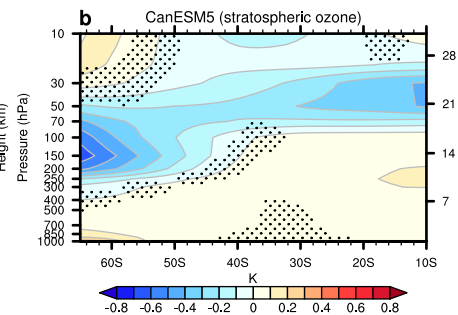
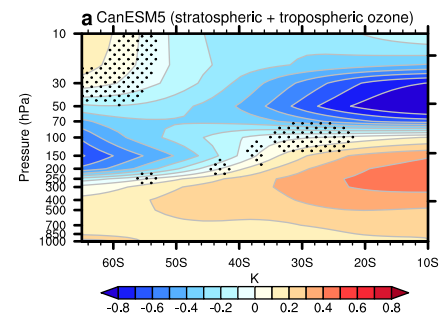


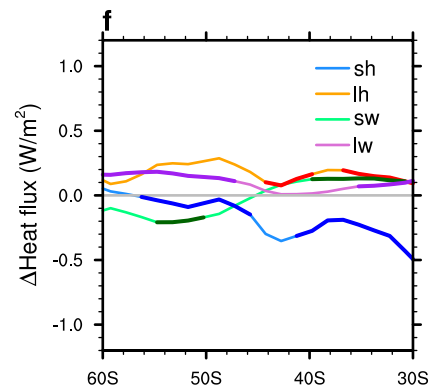
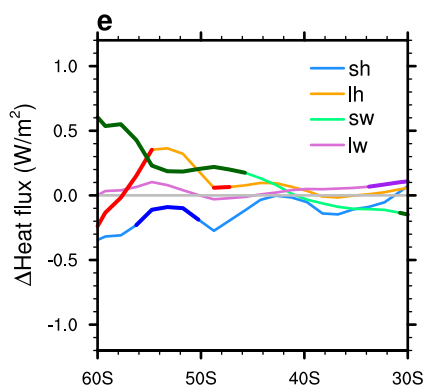
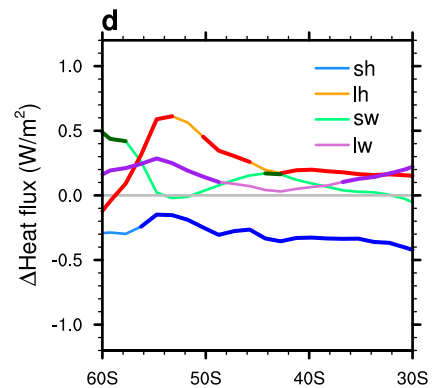
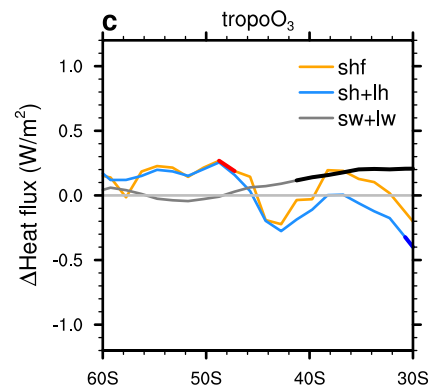
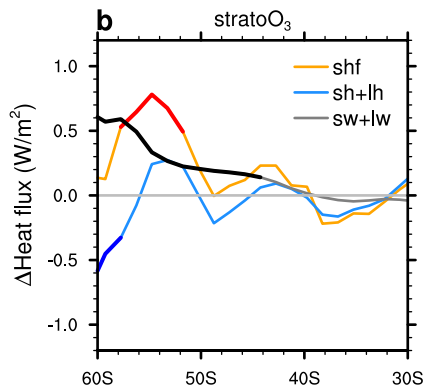
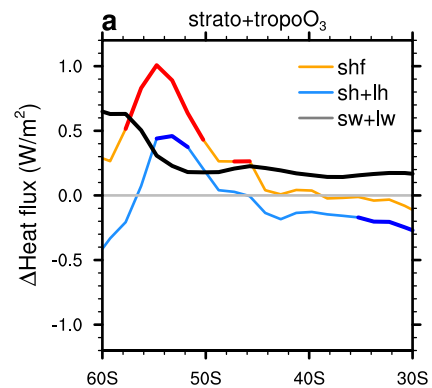


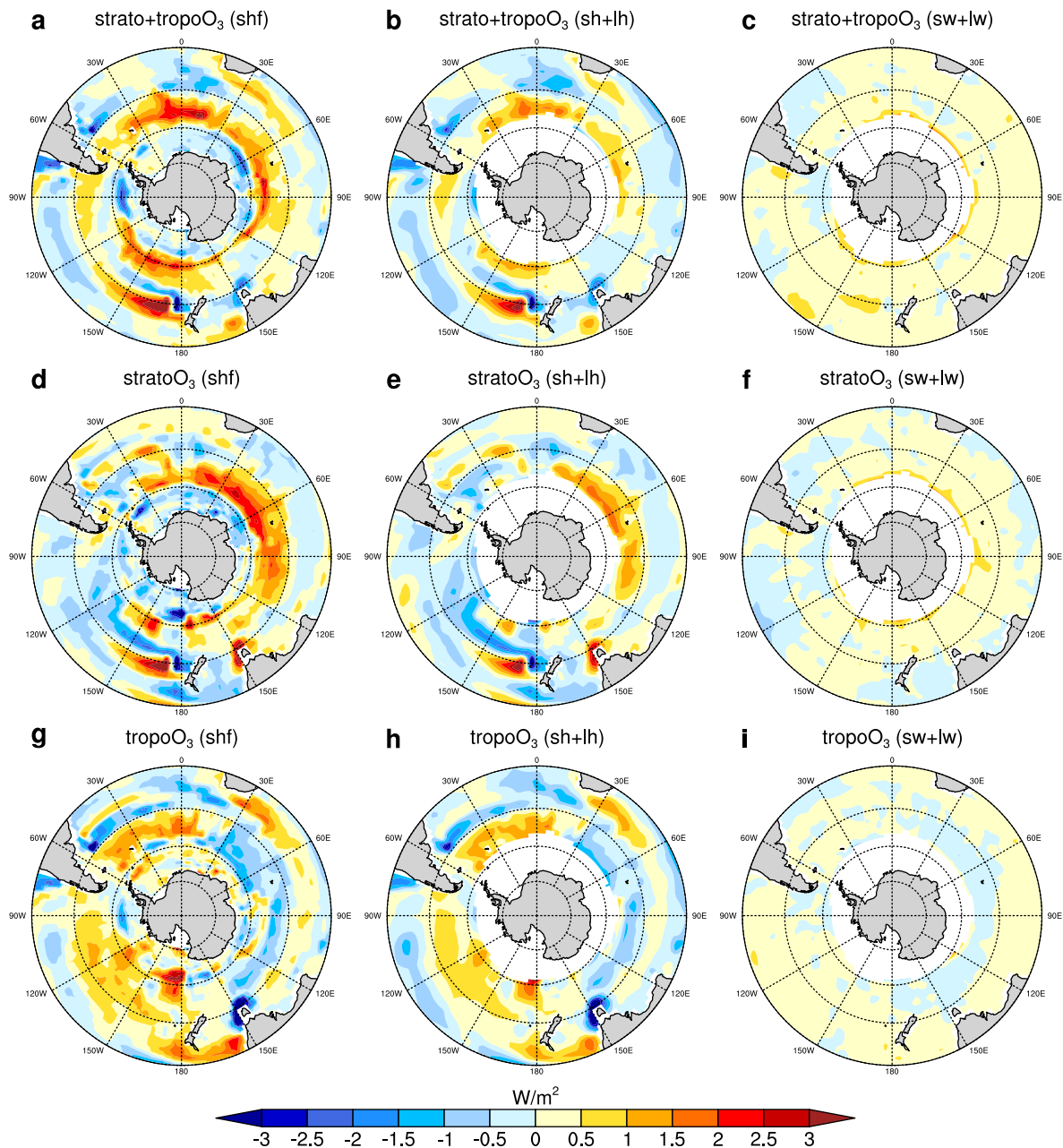


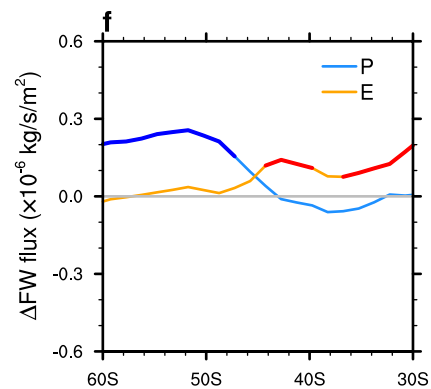
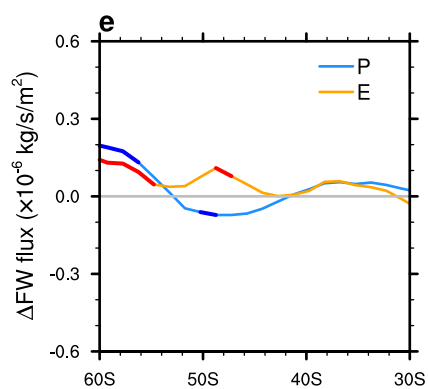
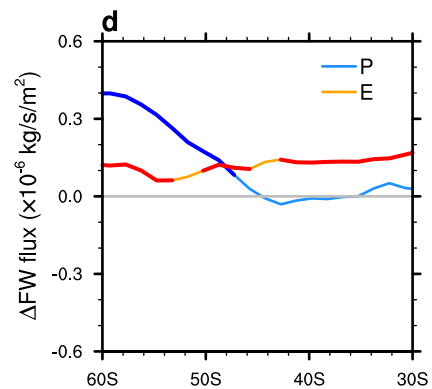
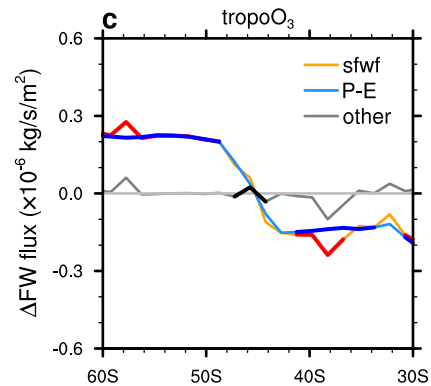
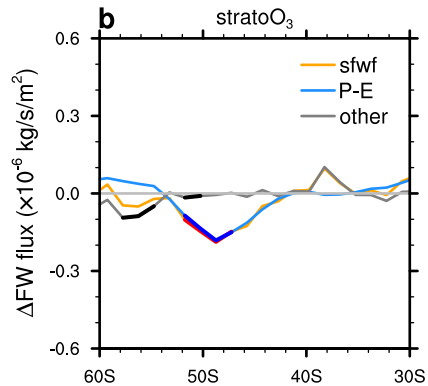
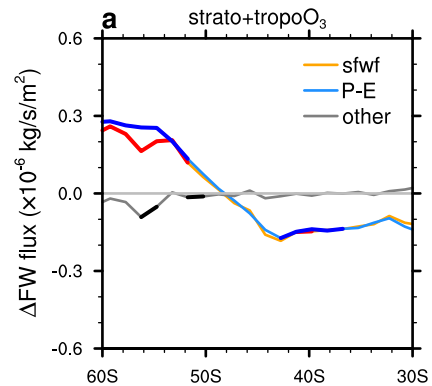


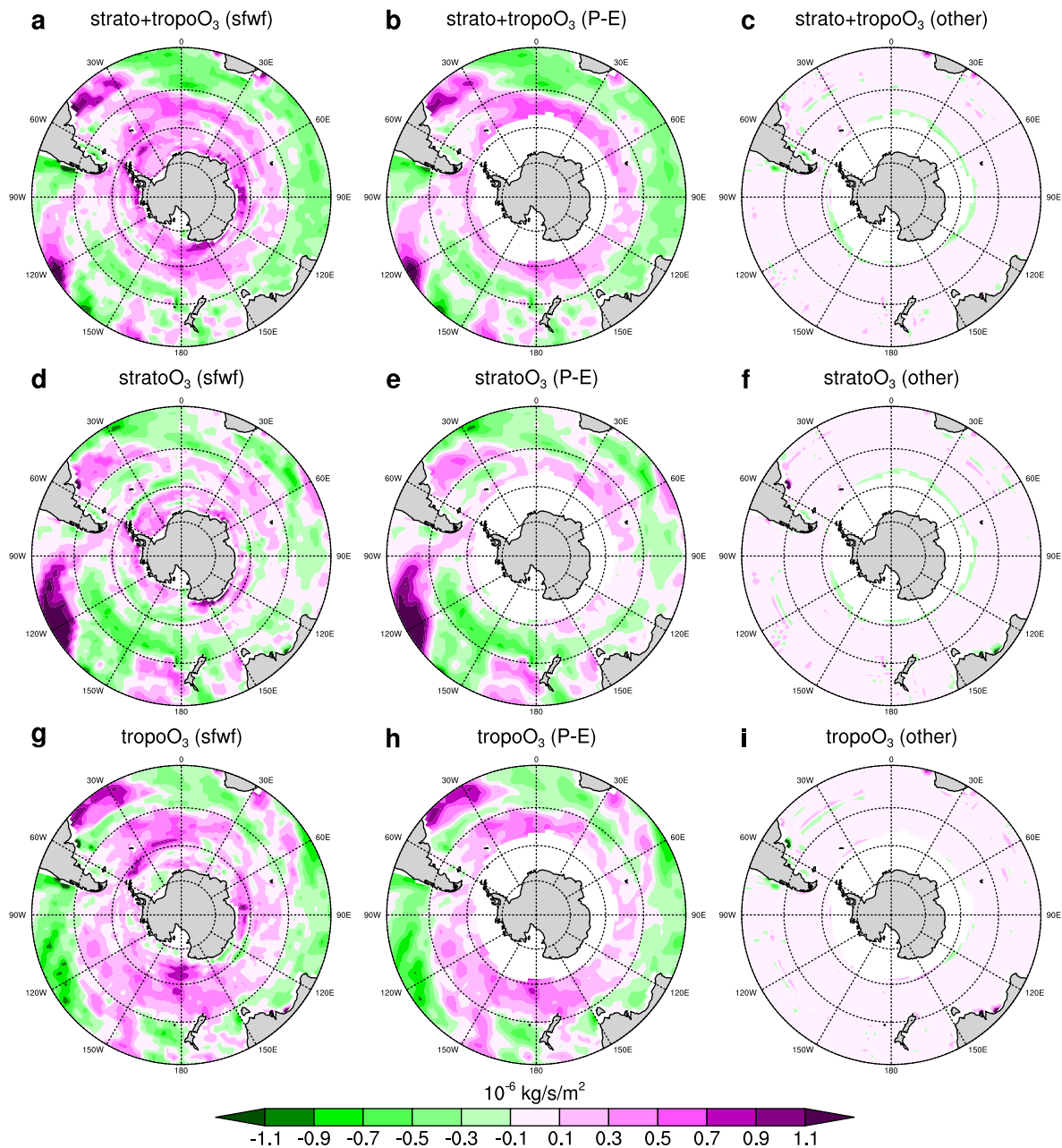


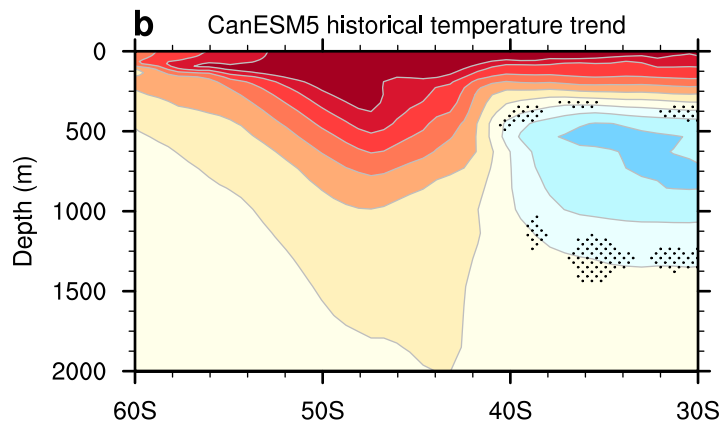
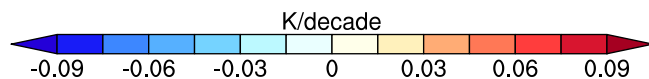
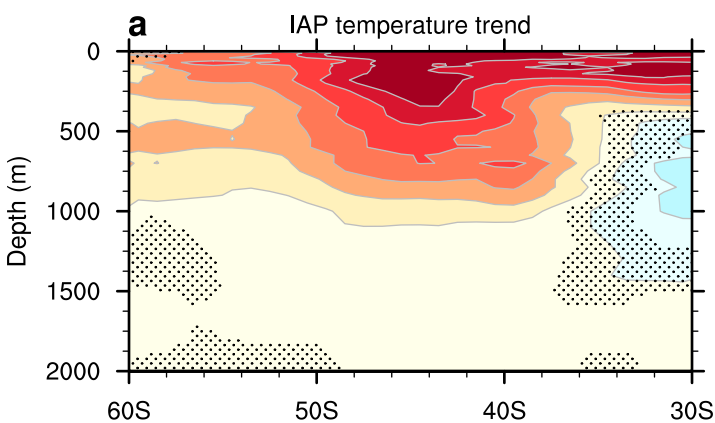


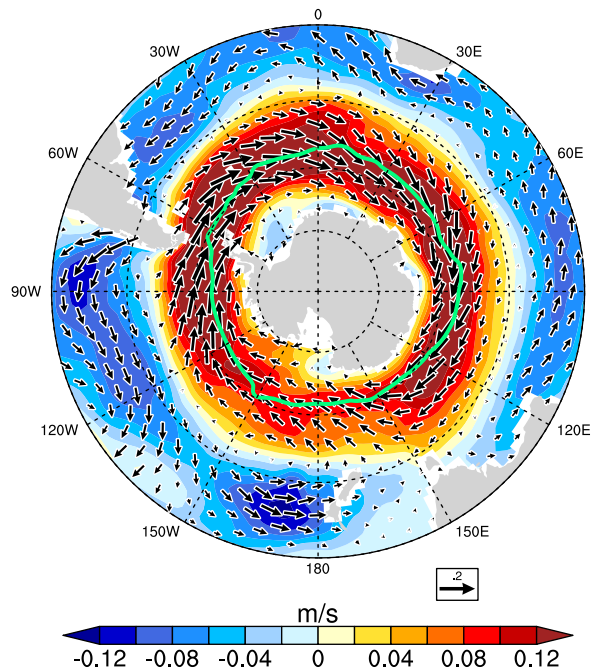
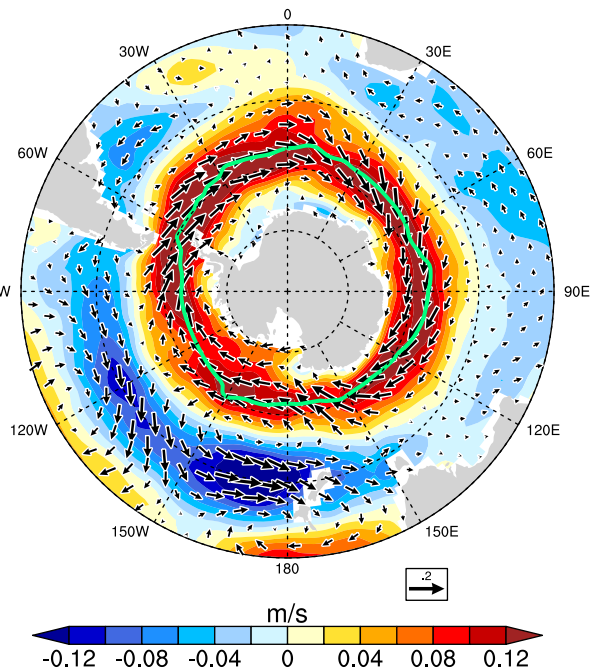
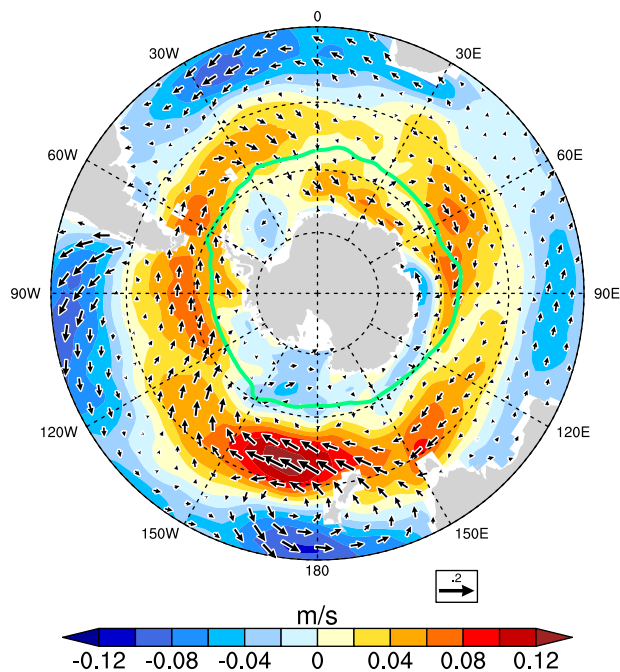










**a** stratospheric + tropospheric ozone**b** stratospheric ozone**c** tropospheric ozone**d**